Allen Wes M. (Orcid ID: 0000-0003-2617-7421)

/

Article type:

Full Article

Title:

Optical palpation for the visualization of tumor in human breast tissue

Authors:

Wes M. Allen, Philip Wijesinghe, Benjamin F. Dessauvagie, Bruce Latham, Christobel M. Saunders, and Brendan F. Kennedy[1,2]

*wes.allen@research.uwa.edu.au

[1]BRITElab, Harry Perkins Institute of Medical Research, QEII Medical Centre, Nedlands and Centre for Medical Research, The University of Western Australia, Perth, Western Australia, 6009, Australia.

[2]Department of Electrical, Electronic & Computer Engineering, School of Engineering, The University of Western Australia, 35 Stirling Highway, Perth, Western Australia, 6009, Australia.

[3]PathWest, Fiona Stanley Hospital, 11 Robin Warren Drive, Murdoch, Western Australia, 6150, Australia.

[4]Division of Pathology and Laboratory Medicine, Medical School, The University of Western Australia, 35 Stirling Highway, Perth, Western Australia, 6009, Australia.

[5]Division of Surgery, Medical School, The University of Western Australia, 35 Stirling Highway, Perth, Western Australia, 6009, Australia.

[6]Breast Centre, Fiona Stanley Hospital, 11 Robin Warren Drive, Murdoch, Western Australia, 6150, Australia.

[7]Breast Clinic, Royal Perth Hospital, 197 Wellington Street, Perth, Western Australia, 6000, Australia.

Keywords:

optical palpation, tactile imaging, breast-conserving surgery, tumor margin assessment, optical coherence tomography

Short title:

Abstract:

Accurate and effective removal of tumor in one operation is an important goal of breast-conserving surgery. However, it is not always achieved. Surgeons often utilize manual palpation to assess the surgical margin and/or the breast cavity. Manual palpation, however, is subjective and has relatively low-resolution. Here, we investigate a tactile imaging technique, optical palpation, for the visualization of tumor. Optical palpation generates maps of the stress at the surface of tissue under static preload compression. Stress is evaluated by measuring the deformation of a contacting thin compliant layer with known mechanical properties using optical coherence tomography. In this study, optical palpation is performed on thirty-four freshly excised human breast specimens. Wide field-of-view (up to ~46 mm × 46 mm) stress images, optical palpograms, are presented from four representative specimens, demonstrating the capability of optical palpation to visualize tumor. Median stress reported for adipose tissue, 4 kPa, and benign dense tissue, 8 kPa, is significantly lower than for invasive tumor, 60 kPa. Additionally, we demonstrate that optical palpation provides contrast consistent with a related optical technique, quantitative micro-elastography. This study demonstrates that optical palpation holds promise for visualization of tumor in breast-conserving surgery.

1. Introduction

Enabling surgeons to accurately assess the surgical margin and/or the breast cavity during breast-conserving surgery may enable more effective removal of tumor [1]. This could potentially reduce the number of patients requiring additional procedures, currently 20−30% [2-5]. A number of techniques have been utilized for intraoperative surgical margin assessment, including frozen section histology, imprint cytology, intraoperative ultrasound

and intraoperative specimen radiography; however, these techniques have not significantly reduced re-excision rates [6-11]. As a result, it is common for many surgeons to rely primarily on manual palpation, *i.e.*, the sense of touch, to locate tumor based on changes in their mechanical properties [12-14]. However, manual palpation is subjective and suffers from low spatial resolution. One method used to determine the spatial resolution of manual palpation, two-point tactile discrimination, reports that the minimum separation at which two points can be resolved by a subject is 1.3 to 5 mm for the fingertip [15, 16]. Another method, grating orientation discrimination, measures the minimum grating spacing, reported to be 0.8 to 1.6 mm, at which subjects can determine orientation [17-19]. Conversely, it has been reported that the fingertip sensitivity extends to the nanoscale under certain conditions, demonstrated by subjects detecting the presence of sinusoidal wrinkle patterns with an amplitude of ~10 nm on substrate surfaces [20]. However, in a clinical setting, the use of surgical gloves degrades both the sensitivity and the resolution of manual palpation [21]. The subjectivity and low spatial resolution of manual palpation limit its efficacy in breast-conserving surgery and restricts surgeons to the identification of gross regions of the tumor [22].

Tactile imaging has been proposed to improve on manual palpation in the pre-operative detection of cancer [23, 24]. In tactile imaging, the subjectivity of manual palpation is removed by translating the sense of touch to a two-dimensional image of stress at the tissue surface, measured using, for example, capacitive or resistive arrays [23-27]. However, as the spatial resolution of tactile imaging is limited by the spacing of sensor elements, typically >1 mm, these techniques provide spatial resolution on a scale similar to manual palpation [25,

28]. An optoelectronic tactile imaging system, proposed for robotics and human-machine interfaces, has demonstrated a resolution of 2.7 μm, using nanowire pressure sensors [29]. However, the small field-of-view, ~100–200 μm, limits its applicability in tumor margin assessment. A number of other optical techniques have also been proposed for tactile imaging [30-34]. In particular, optical palpation, based on optical coherence tomography (OCT), has the potential to estimate stress at the surface of tissue at a resolution suitable for tumor margin assessment [32, 33]. It has previously been demonstrated that optical palpation can generate images of stress, referred to here as optical palpograms, with a lateral resolution of 160 to 390 μm [32, 33]. Furthermore, a recently developed extension of optical palpation, computational optical palpation, has demonstrated a resolution of 15–25 μm, over a field-of-view of 7 × 7 mm, achieved by incorporating finite-element methods in the computation of stress [35].

To perform optical palpation, a thin compliant silicone layer is compressed (preloaded), between a specimen and an imaging window. The deformed thickness of the layer is measured using an OCT system, from which strain, *i.e.*, the change in thickness divided by the original thickness, at each lateral position in the layer is calculated [32, 33]. Stress is determined by relating the strain to the known stress-strain relationship of the layer under the assumption that the stress field within the layer is uniform and uniaxial, and the friction of the layer interfaces is low [33]. An advantage of optical palpation over many tactile imaging techniques is that the compliant layer deforms to accommodate the rough surface invariably present in excised biological tissue: an important attribute for imaging surgical

margins. A further advantage of optical palpation is that, in addition to optical palpograms, 3D-OCT images of the tissue micro-architecture are generated. OCT images provide excellent contrast between adipose tissue and dense tissue and, additionally, can delineate certain imaging artifacts, such as those caused by air bubbles, aiding in the interpretation of stress. For this reason, we present optical palpograms here as semi-transparent overlays on *en face* OCT images.

Optical palpation, as with all tactile imaging techniques, provides contrast related to variations in the underlying mechanical properties of tissue. In optical palpograms, elevated regions of stress indicate stiffer underlying features. If the preload is kept approximately constant between samples, stress may be used to distinguish tissue types, as we report in this paper. However, stress is a qualitative measurement of elasticity, and the measured stress is proportional to the preload. A related technique, quantitative micro-elastography (QME), reports tissue elasticity, defined here as the slope of the stress-strain curve at the point of preload, *i.e.*, the tangent modulus [36, 37]. Despite the quantification of elasticity provided by QME, in this study, we suggest that optical palpation may provide a less complex and more cost-effective solution for margin assessment in a large subset of tumors, particularly in invasive tumors, which tend to present as larger regions of tumor.

In this paper, we present a feasibility study assessing the use of optical palpation to identify tumor in freshly excised human breast tissue. We provide four representative wide-field (up to ~46 × 46 mm) optical palpograms from a study performed on thirty-four specimens from patients undergoing mastectomy or breast-conserving surgery. The images

presented demonstrate contrast in adipose, uninvolved stroma, invasive tumor, and ducts involved by high-grade ductal carcinoma *in situ* (DCIS). In addition, we provide a comparison of optical palpation and QME. Finally, we perform statistical analysis on a subset of specimens (n = 19) and report that the median stress for adipose tissue (4 kPa) and uninvolved dense tissue (8 kPa) is significantly lower than for invasive tumor (60 kPa). The results presented here demonstrate the potential of optical palpation in the visualization of tumor in freshly excised human breast tissue.

2. Materials and Methods

2.1. Imaging system,

The imaging system comprises four main components: a compliant layer, an OCT system, a specimen mounting mechanism and a wide-field translation system (**Figure S1a** Supporting Information [38]). The system is configured such that optical palpation and QME results are generated from the same OCT datasets.

The compliant layers used in this study were formulated using two-component room-temperature-vulcanizing silicone, Elastosil P7676 (Wacker GmbH, Germany), with a 1:1 (Cross-linker : Catalyst) mixing ratio. The elastic modulus of the compliant layers is ~6.4 kPa at 5% strain [39]. The thickness of the layers, (500 to 650 μm) is measured before testing to allow subsequent calculation of layer strain, described in Section 2.2. The OCT system is based on a Telesto II spectral-domain OCT system (TEL220C1, Thorlabs Inc., USA). The system uses a superluminescent diode light source with a central wavelength of 1300 nm and a bandwidth of >170 nm. The OCT sensitivity is 98 dB for an A-line rate of 76 kHz. The A-line rate used in this study is ~71 kHz. The lens used in this study (LSM04, Thorlabs Inc.,

USA) has a numerical aperture of 0.04. The measured full width at half maximum axial and lateral OCT resolutions are 5.5 μm (in air) and 13 μm, respectively.

The specimen mounting mechanism (Figure S1b Supporting Information [38]) comprises an imaging window, a compression plate, a laboratory jack and an annular piezoelectric actuator (required for QME). The compression plate is mounted on three load cells (LSB200, Futek Inc., USA), which in turn are mounted on a motorized laboratory jack (MLJ050/M, Thorlabs Inc., USA). The 75-mm diameter imaging window (84-359, Edmund Optics Inc., USA) is rigidly affixed to the piezoelectric actuator (Piezomechanik GmbH, Germany). The actuator has an aperture of 65 mm and a maximum stroke of 9.5 μm. Before scanning, the specimen is placed on the compression plate, and saline is applied to keep it hydrated during testing (the saline also lubricates the layer-specimen interface). A layer is then placed on the specimen, and silicone fluid (AK50, Wacker GMBH, Germany) is used to lubricate the top surface of the layer. The laboratory jack applies a preload strain of approximately 15–25% of the maximum undeformed thickness of the specimen, compressing the specimen and layer against the imaging window. This preload range, determined empirically, ensures sufficient contact between the specimen, layer and imaging window while minimizing the influence of the non-linear stress-strain relationship of tissue. Following the application of preload, a one-minute delay is allowed to reduce the impact of viscoelastic creep [40]. The OCT system is configured in a common-path mode with the interface between the imaging window and the compliant layer acting as the reference reflector [37].

Translations stages (NRT100/M, Thorlabs Inc., USA) move the specimen mounting mechanism relative to the OCT scan head to generate wide-field images, up to ~46 × 46 mm, by acquiring individual OCT volumes (termed sub-volumes) which are mosaicked in post-processing. The travel range of the translation stages is 100 mm and the velocity and acceleration are 30 mm s^{-1} and 30 mm s^{-2}, respectively. Sub-volumes, measuring 16 × 16 × 3.5 mm, are acquired with 808 A-lines per B-scan and 2,424 B-scan pairs per sub-volume. B-scan pairs comprise two B-scans in the same location; the first B-scan is acquired with only the preload compression applied, **Figure 1**a(ii), the second B-scan (required for QME) is acquired with an additional micro-scale compression applied by the actuator, Figure 1a(iii) [37]. Only the first OCT B-scan in each pair, *i.e.*, without the actuation compression applied, at each spatial location is required for optical palpation signal processing, Section 2.2.1., provided the undeformed thickness of the layer is known. To enable a comparison of optical palpation and QME in this study, the two measurements were generated from the same OCT dataset.

2.2. Signal processing

2.2.1. Signal processing for optical palpation

In optical palpation signal processing, the deformed thickness of the layer, resulting from preload, at each lateral position is measured by detecting the layer-specimen interface using a Canny-based edge detection algorithm on the OCT B-scans, Figure 1a(ii) [41]. Smoothing is performed on the detected edge using a Hampel-based median filter, with a window of ~80 μm, to remove outliers. The layer preload strain, $\mu_{layer,P}$, is calculated by dividing the change in thickness by the original thickness. The layer preload stress, $\tilde{A}_{layer,P}$, is estimated by

relating the layer preload strain to the stress-strain response of the layer, E_{layer}, under the assumption that the stress field in the layer is uniform and uniaxial, and the friction at the layer interfaces is low, Figure 1b(i) [33]. Figure 1b(ii), shows an *en face* optical palpogram demonstrating elevated stress contrast provided by a stiff inclusion, $\tilde{A}_1$, surrounded by a softer bulk material, $\tilde{A}_2$.

2.2.2. Signal processing for QME

In QME, first, the layer preload stress is determined by following the same steps as optical palpation. Then, local displacement, arising from actuation, is calculated for each lateral and axial location in the OCT field-of-view from the measured phase-difference between OCT B-scans in pairs [40]. The layer local strain, $\mu_{layer,L}$, is calculated by dividing the measured displacement at the layer-specimen interface by the undeformed layer thickness, Figure 1a(iii) [37]. The layer local stress, $\tilde{A}_{layer,L}$, is estimated by relating the layer local strain to the known stress-strain response of the layer, E_{layer}, Figure 1c(i) [37]. The sample local strain, $\mu_{sample,L}$, defined as the gradient of axial displacement with respect to depth, is calculated using weighted least squares linear regression, over a fitting range of 100 µm [40]. Sample elasticity, E_{sample}, is estimated at each spatial location in the sample by dividing the 2D local stress in the layer by the 3D local strain in the sample, under the assumption that the local stress in the layer acts uniformly with depth [37]. Figure 1c(ii), shows an *en face* quantitative micro-elastogram of the stiff inclusion presented in Figure 1b(ii).

2.2.3. En face image generation

Wide-field *en face* images are generated by mosaicking *en face* sub-images with an overlap of 1 mm to ensure accurate alignment can be achieved and to minimize areas of low OCT intensity due to coherence gate curvature [36]. Wide-field *en face* OCT images are generated (at a single pixel depth) ~100 μm below the layer-specimen interface. Optical palpograms are generated by overlaying stress, with an opacity of 70%, on grayscale OCT images using image-processing software (GNU Image Manipulation Program, v2.8.22). Stress is presented in false color, on a log scale. Stress values corresponding to regions of non-contact between the layer and the specimen are not presented in optical palpograms. Quantitative micro-elastograms are also generated as overlays on OCT images, however, as the accuracy of elasticity is low in regions of low OCT signal-to-noise ratio, such as in adipose tissue, elasticity is overlaid in regions of dense tissue only [40]. A custom binary segmentation algorithm is used to identify regions of dense tissue and to produce binary masks. Due to the complex mechanical structure of the tissue, in some cases, negative elasticity is estimated in QME [36]. As negative elasticity is not physically meaningful, these pixels are also segmented from the final image. Elasticity is presented in false color, on a log scale. Quantitative micro-elastograms are generated by applying the binary mask to elasticity and overlaying, with an opacity of 100%, on grayscale OCT images.

2.3. Clinical protocol

Specimens were obtained from patients undergoing either mastectomy or breast-conserving surgery at Fiona Stanley Hospital, Western Australia. Informed consent was obtained from patients, and the ethics for this research project have been approved by the South Metropolitan Health Service, Western Australia, Human Research Ethics Committee and the

Fiona Stanley Hospital Human Research Ethics Committee (FSH-2015-032). In this study, mastectomy specimens from seven patients and breast-conserving surgery specimens from twenty-seven patients were imaged. The inclusion of mastectomy specimens allows presentation of *en face* images in the same plane as scanned digital micrographs of the histology slides, thus, providing direct validation of the contrast in optical palpograms. Following surgery, specimens were transferred from the operating theater to the anatomical pathology laboratory immediately post-operatively.

2.3.1. Pathology handling of mastectomy specimens

Mastectomy specimens were serially sectioned following standard protocols at Fiona Stanley Hospital. Direct visualization and manual palpation were utilized to identify an area of interest. To provide a specimen with suitable dimensions for imaging, this area was excised from the mastectomy. Following imaging, the perimeter of the extracted specimen was inked to allow subsequent re-approximation of the specimen, which required dissection into smaller pieces to fit within cassettes for histopathology processing. The cassettes were fixed in 10% neutral-buffered formalin for at least 24 hours.

2.3.2. Pathology handling of breast-conserving surgery specimens

Breast-conserving surgery specimens were imaged with no further dissection, to mimic the clinical scenario of margin assessment. Two types of breast-conserving surgery were imaged, diagnostic open biopsies for benign fibroadenomas and wide-local excisions for cancer. As the status of the surgical margin of diagnostic open biopsies is not reported, the orientation of the specimen was not indicated. In the case of wide-local excisions, the orientation of the specimens is indicated by the placement of sutures and clips during the surgical procedure,

visible in **Figure 3**a. During imaging, the orientation of wide-local excisions was recorded for later co-registration of digital micrographs. Following imaging, wide-local excisions were inked for orientation in histopathology. Both types of breast-conserving surgery specimens were fixed in 10% neutral-buffered formalin for at least 24 hours. The specimens were then serially sectioned, with areas of tumor, close-by margins and other areas of interest sampled and placed in cassettes for histopathology processing.

2.3.3. Histopathological processing

Cassettes described in the previous sub-sections were processed into paraffin blocks according to standard practice. Paraffin blocks were sectioned and stained with hematoxylin and eosin. The histology slides were scanned at 40× magnification to generate digital micrographs for subsequent analysis by a pathologist. In mastectomy specimens, the digital micrographs were manually stitched to enable co-registration with wide-field *en face* OCT images, optical palpograms and, in **Figure 5**, quantitative micro-elastograms. In diagnostic open biopsy specimens, the orientation and location of the digital micrographs in relation to OCT images and optical palpograms were unknown, and thus the images were compared to representative digital micrographs of the specimen. In wide-local excision specimens, the orientation of digital micrographs is in the plane orthogonal to *en face* OCT images and optical palpograms. In these cases, as the position of the micrograph relative to the specimen boundaries was known, the approximate location of digital micrographs in relation to OCT images and optical palpograms was determined and indicated in *en face* images.

3. Results

In **Figure 2**-4, we present OCT images and optical palpograms of human breast specimens, freshly excised from patients undergoing mastectomy or breast-conserving surgery. To provide a comparison of mechanical contrast in optical palpation and QME, in Figure 5, we present OCT images, optical palpograms and quantitative micro-elastograms of a mastectomy specimen. In **Figure 6**, we present an analysis comparing the stress for three tissue types: adipose tissue, uninvolved dense tissue, and invasive tumor.

Figure 2 provides an example of the additional contrast in invasive tumor provided by optical palpation compared to OCT alone. The images were acquired from a 59-year-old patient undergoing a mastectomy. A photograph of the preloaded specimen, measuring ~45 × 45 mm, is shown in Figure 2a. Analysis of the digital micrographs, Figure 2b and 2c, show that the specimen comprised uninvolved stroma (S), invasive tumor (T) and adipose tissue (A). Magnified in Figure 2c is a region of tissue containing invasive tumor, uninvolved stroma, and clusters of adipose cells. Adipose tissue can be identified in the wide-field OCT image, Figure 2d, by its distinctive honeycomb structure arising from spherical hyposcattering fat reservoirs surrounded by hyperscattering cell walls [42]. The magnified OCT image, Figure 2f, corresponds to the region of magnified histology in Figure 2c. The OCT intensity appears slightly higher in uninvolved stroma, however, the contrast between uninvolved stroma and the invasive tumor is subtle. The wide-field optical palpogram, Figure 2e, shows a region of high stress in the center of the specimen corresponding to the bulk of invasive tumor in the specimen. The magnified optical palpogram, Figure 2g, shows elevated stress, >60 kPa, corresponding to the invasive tumor. By contrast, uninvolved stroma shows low stress ranging from 10−15 kPa. The results shown in Figure 2 demonstrate how mechanical contrast provided by optical palpograms complements the contrast provided by OCT alone and aids in delineating invasive tumor and uninvolved stroma.

In Figure 3 we demonstrate the ability of optical palpation to detect an involved margin in a breast-conserving surgery specimen excised from a 64-year-old patient. A photograph of the superior margin of the specimen, measuring 70 × 70 mm, is shown in Figure 3a. A digital micrograph from a section of the superior margin is shown in Figure 3b.

The digital micrograph is orthogonal to the *en face* OCT image and wide-field optical palpogram, as illustrated in Figure 3b. Histopathological analysis of the digital micrograph revealed invasive tumor (T) within 300 μm of the margin. This micrograph also shows adipose tissue (A) and uninvolved stroma (S). Red dashed lines indicate the approximate location of the digital micrograph in Figure 3c-3f. The wide-field OCT image, Figure 3c, shows that the superior margin contains a mix of adipose tissue and dense tissue. The magnified OCT image, Figure 3e, shows heterogeneous intensity, indicative of invasive tumor [43]. In the corresponding region of the wide-field optical palpogram, Figure 3d, regions with stress greater than 70 kPa are visible, also indicative of invasive tumor as demonstrated in Figure 2. Benign stroma and adipose tissue exhibit low stress in the optical palpogram. The magnified optical palpogram, Figure 3f, shows in detail the region of invasive tumor. An artifact, in an area where the specimen surface topology prevented contact between the specimen and layer, is visible in the *en face* images (L). The high stress in the optical palpogram more clearly delineates the tumor from the surrounding dense tissue than the heterogeneous intensity in the OCT image.

In **Figure 4**, we present an optical palpogram demonstrating that low, homogeneous stress is indicative of benign dense tissue. The images were acquired from the open diagnostic biopsy of a benign fibroadenoma excised from a 29-year-old patient. A photograph of the specimen, measuring ~30 × 25 mm, is presented in Figure 4a. Representative histology of this specimen is presented in Figure 4b, as the orientation of diagnostic open biopsies is not reported. Analysis of the digital micrograph identified a well-circumscribed benign fibroadenoma (FA) composed of compressed and elongated ducts within dense fibrous stroma

with surrounding adipose tissue (A). In Figure 4c, we present the wide-field OCT image of the benign fibroadenoma, which appears as a solid region of highly scattering, dense tissue. In the magnified OCT image, Figure 4e, we see hyperscattering luminal and tubular structures with highly scattering interiors, indicative of ducts involved by DCIS. However, the low homogeneous stress, 5−10 kPa, in the wide-field optical palpogram, Figure 4d, indicates that this specimen comprises uninvolved dense tissue, consistent with Figure 2. The magnified optical palpogram, Figure 4f, shows subtle changes in stress, corresponding to variations in elasticity within the fibroadenoma. An artifact (L), caused by the layer sticking to the imaging window as the specimen was positioned, is visible in wide-field *en face* images, Figure 4c and 4d.

In Figure 5, a comparison of the mechanical contrast provided by optical palpograms and quantitative micro-elastograms is provided. The images were acquired from tumor excised from a 77-year-old patient undergoing a mastectomy. A photograph of the scanned region of the specimen, measuring 40 × 30 mm, is shown in Figure 5a. Three digital micrographs were manually stitched and are shown in Figure 5b. The specimen contains numerous ducts involved by DCIS (D) and small regions of adipose tissue (A). In Figure 5c, we present magnified histology of a region of tissue comprising ducts involved by DCIS containing focal calcifications (FC). The wide-field OCT image, Figure 5d, shows a central region of dense tissue and small regions of adipose tissue. In the magnified OCT image, Figure 5g, luminal structures of ducts with hyposcattering interiors are visible. However, it is ambiguous if the ducts are benign or involved by DCIS [44]. The wide-field optical palpogram, Figure 5e, shows a central region of high stress corresponding to DCIS. The

magnified optical palpogram, Figure 5h, shows higher stress resulting from the stiff calcifications, demonstrating the potential for optical palpation to identify ducts involved by high-grade DCIS with focal calcifications. The wide-field quantitative micro-elastogram, Figure 5f, shows high elasticity in the center of the specimen corresponding to DCIS. Comparison of the magnified optical palpogram, Figure 5h, and quantitative micro-elastogram, Figure 5i, demonstrates the corresponding mechanical contrast provided by optical palpation and QME, respectively. At this magnified scale, it is apparent that quantitative micro-elastograms provide a higher mechanical resolution (For additional information, please refer to the Supporting Information [38]). This is visible in features exhibiting a sharper change in measured mechanical properties, such as duct walls (W), which are more readily identified by patterns in quantitative micro-elastograms than in optical palpograms, in which the duct walls are primarily delineated by OCT contrast. In Figure 5i, the elasticity in some regions is masked due to negative elasticity. However, the optical palpogram, Figure 5h, shows mechanical contrast in this region.

Figure 6 presents a comparison of the stress across three tissue types in a larger subset of specimens than presented in Figure 2-4. Due to the surface topology of some specimens, sufficient contact was achieved with a preload strain outside the target 15–25% range. As the stress estimated is dependent on the preload, to reduce the influence of a variable preload in this analysis, only specimens with a preload strain between 15–25% were included for this analysis (n = 19). For each specimen, a minimum of one region (1 mm^2) was selected and the average stress recorded. Selected regions contained either adipose tissue, uninvolved dense

tissue or invasive tumor (within 2 mm of the margin). In specimens containing invasive tumor (n = 6), up to three non-overlapping regions were selected. The total number of regions of adipose tissue and uninvolved dense tissue was limited to match the number of invasive tumor regions (n = 16). The median (interquartile range) stress for adipose tissue, uninvolved dense tissue, and invasive tumor are 4 kPa (3−5 kPa), 8 kPa (6−12 kPa) and 60 kPa (25−68 kPa), respectively. Stress is not significantly different between adipose tissue and uninvolved dense tissue (n = 16; p = 0.15; Welch's t-test). However, the stress is significantly higher for invasive tumor in comparison to both adipose tissue (n = 16; $p = 1.7e^{-6}$; Welch's t-test) and uninvolved dense tissue (n = 16; $p = 4.1e^{-5}$; Welch's t-test).

4. Discussion

In this paper, we have demonstrated that optical palpation can visualize tumor by mapping stress at the surface of freshly excised human breast tissue under compression. We have presented optical palpograms of four specimens, chosen from the thirty-four specimens imaged, to provide representative contrast in a range of tissue types. These representative results demonstrate that optical palpograms complement OCT by providing additional contrast based on the mechanical properties of tissue. This feasibility study represents an important step towards clinical translation of optical palpation for tumor margin assessment. The methods described here could provide the basis for larger clinical studies to determine the diagnostic accuracy of optical palpation for tumor margin assessment. Such studies would enable a better understanding of other factors that may affect the mechanical properties of tissue, for example, breast density or patient age, which were beyond the scope of this current feasibility study.

Statistical analysis performed in this study has shown that tumor exhibits median stress of 60 kPa, higher than that of adipose and stroma, in cases when the preload was controlled between 15–25%. The elevated stress, which is sensitive to the underlying elasticity of features in tissue, measured for invasive tumor in this study is consistent with QME studies; where it was shown that invasive tumor exhibits elevated elasticity in comparison to benign dense tissue [36, 37]. Stress is a qualitative measurement; therefore, the measured stress in the layer is proportional to the preload applied. Furthermore, as breast tissue is a hyperelastic material, the stress-strain relationship is non-linear. Therefore, the rate of change of stress will increase at higher preloads. However, in situations where the preload strain cannot be readily controlled, for example in an *in vivo* setting, the relative contrast between the stresses of features in optical palpograms can also be considered when interpreting optical palpograms.

There are some potential advantages of optical palpation over QME for tumor margin assessment. Optical palpation requires a less complex imaging system, as there is no actuator synchronized to the OCT system. Instead, to generate mechanical contrast, optical palpation relies only on the contact force provided by preload. Consequently, optical palpation may be more practical to translate into a form factor suitable for *in vivo* imaging of the breast cavity [32, 45]. Optical palpation may also prove more robust in generating mechanical contrast in highly scattering tissue, such as blood. Unlike QME, optical palpation does not rely on scattering from within the specimen to generate mechanical contrast; it requires only a measurement of the compliant layer thickness.

Additionally, as optical palpation does not require high OCT sensitivity to detect the layer-specimen interface, and it does not require phase-sensitive detection, it is well suited to low-cost OCT systems, a further advantage for clinical translation. Optical palpation measurements also have the potential to be acquired in less time than QME measurements as it is not necessary to acquire pairs of B-scans in each. Finally, we anticipate that by mimicking the sense of touch, a tool that surgeons routinely use to assess tissue, optical palpation may provide images that can prove more intuitive to interpret than other forms of intraoperative imaging. However, the significant advantages of QME over optical palpation are the quantification of elasticity [37], the ability to perform depth sectioning of mechanical contrast, up to ~1 mm [36], and higher spatial resolution (which is discussed in the Supporting Information [38]).

In addition to the underlying elasticity of features in tissue, the surface stress is further sensitive to the size and depth of these features. To maximize the diagnostic accuracy of optical palpation in margin assessment, it is important to avoid erroneously identifying high stress caused by a stiff feature far below the surface as tumor at the surgical margin. An advantage of optical palpation in this regard is that 3D-OCT images are also generated of the tissue micro-architecture. Presenting optical palpograms as semi-transparent overlays on *en face* OCT images aids in the interpretation of mechanical contrast and helps to avoid such erroneous interpretation of optical palpograms. In addition, we expect that optical palpograms from deep stiff features will manifest differently to those from shallow stiff features. In the case of a feature far from the margin, we would expect to see a gradual spatial increase in stress compared to a sharper increase in stress for stiff features near the surface. Other tactile

imaging techniques have proposed inverse and semi-empirical methods to generate 3D images [23, 24]. These methods could be translated to optical palpation to provide depth-resolved mechanical contrast.

Extension of computational optical palpation to the results presented here has the potential to more accurately characterize the stress field in the layer [35]. Such methods would enable us to remove the need for the assumptions that the stress field within the layer is uniform and uniaxial, and the interface friction is low; this would result in a significant increase in resolution of optical palpograms [35]. Preliminary work indicated that additional development is required to perform computational optical palpation over the field-of-views presented in the current study, due to discontinuities in the measured layer thickness. Such discontinuities arise from performing the edge detection across wide fields-of-view on uneven surfaces and the mosaicking of sub-images. These discontinuities could be overcome by employing edge detection methods that impose local continuity, such as active contours, or by using softer contact models in the finite element method. Proposed computation methods could also be incorporated to better characterize the stress field in mechanically heterogeneous tissue for QME measurements by developing iterative solutions to the inverse elasticity problem [46]. However, the relative contrast between uninvolved stroma and tumor demonstrated in this feasibility study indicate that the algebraic method of determining stress, used here, provides sufficient resolution and contrast for tumor margin assessment.

5. Conclusion

We have demonstrated the ability of optical palpation to visualize tumor in freshly excised human breast tissue. The optical palpograms presented here have demonstrated increased

contrast over OCT alone in benign dense tissue, high-grade *in situ* tumor and invasive tumor. We have presented images indicating the suitability of optical palpation to detect an involved margin in a clinically relevant wide-local excision specimen. We have also demonstrated the corresponding mechanical contrast in optical palpograms and quantitative micro-elastograms. We have performed analysis across three tissue types, comparing the median stress for adipose tissue, 4 kPa, benign dense tissue, 8 kPa and invasive tumor, 60 kPa. Optical palpation provides a number of advantages over QME that may aid in the clinical translation of the technique, including providing a less complex and more cost-efficient imaging system and mapping a parameter that more closely mimics manual palpation. This feasibility study has demonstrated the potential for optical palpation in the visualization of tumor and represents an important step towards clinical translation of optical palpation for tumor margin assessment.

Acknowledgments

The authors acknowledge Dr. Kelsey Kennedy, Dr. Qi Fang, Dr. Lixin Chin, Dr. Andrea Curatolo, Mr. Rowan Sanderson, Ms. Lucinda Watts, Dr. Renate Zilkens and Dr. Synn Lynn Chin for assistance with clinical scanning. We also thank Mr. Matt Hepburn for fruitful discussions regarding mechanical resolution. The authors acknowledge the facilities, and the scientific and technical assistance of the Australian Microscopy & Microanalysis Research Facility at the Centre for Microscopy, Characterization & Analysis, The University of Western Australia, a facility funded by the University, State and Commonwealth Governments.

Funding

This work was supported by research grants from the Australian Research Council, the Department of Health, Western Australia and the Cancer Council, Western Australia; a research contract with OncoRes Medical; and a scholarship from the William and Marlene Schrader Trust of The University of Western Australia.

Conflict of Interest

Brendan F. Kennedy, Bruce Latham, and Christobel M. Saunders hold shares in a startup company, OncoRes Medical, developing optical coherence elastography for surgical applications. Brendan F. Kennedy receives research funding from this company. The other authors declare no conflicts of interest related to this article.

References

[1] L. Jacobs, *Positive margins: The challenge continues for breast surgeons.* Ann. Surg. Oncol., 2008. **15**(5): p. 1271-1272.

[2] H. Ballal, D. B. Taylor, A. G. Bourke, B. Latham, and C. M. Saunders, *Predictors of re-excision in wire-guided wide local excision for early breast cancer: A Western Australian multi-centre experience.* ANZ J. Surg., 2015. **85**(7-8): p. 540-545.

[3] R. Jeevan, D. Cromwell, M. Trivella, G. Lawrence, O. Kearins, J. Pereira, C. Sheppard, C. Caddy, and J. Van Der Meulen, *Reoperation rates after breast conserving surgery for breast cancer among women in England: Retrospective study of hospital episode statistics.* BMJ Brit. Med. J., 2012. **345**: p. e4505.

[4] E. D. Kurniawan, M. H. Wong, I. Windle, A. Rose, A. Mou, M. Buchanan, J. P. Collins, J. A. Miller, R. L. Gruen, and G. B. Mann, *Predictors of surgical margin status in breast-conserving surgery within a breast screening program.* Ann. Surg. Oncol., 2008. **15**(9): p. 2542-2549.

[5] B. J. Adams, C. K. Zoon, C. Stevenson, P. Chitnavis, L. Wolfe, and H. D. Bear, *The role of margin status and reexcision in local recurrence following breast conservation surgery.* Ann. Surg. Oncol., 2013. **20**(7): p. 2250-2255.

[6] N. Cabioglu, K. K. Hunt, A. A. Sahin, H. M. Kuerer, G. V. Babiera, S. E. Singletary, G. J. Whitman, M. I. Ross, F. C. Ames, and B. W. Feig, *Role for intraoperative margin assessment in patients undergoing breast-conserving surgery.* Ann. Surg. Oncol., 2007. **14**(4): p. 1458-1471.

[7] K. Esbona, Z. Li, and L. G. Wilke, *Intraoperative imprint cytology and frozen section pathology for margin assessment in breast conservation surgery: A systematic review.* Ann. Surg. Oncol., 2012. **19**(10): p. 3236-3245.

[8] T. Olson, J. Harter, A. Munoz, D. Mahvi, and T. Breslin, *Frozen section analysis for intraoperative margin assessment during breast-conserving surgery results in low rates of re-excision and local recurrence.* Ann. Surg. Oncol., 2007. **14**(10): p. 2953-2960.

[9] M. Bakhshandeh, S. O. Tutuncuoglu, G. Fischer, and S. Masood, *Use of imprint cytology for assessment of surgical margins in lumpectomy specimens of breast cancer patients.* Diagn. Cytopathol., 2007. **35**(10): p. 656-659.

[10] L. F. Smith, I. T. Rubio, R. Henry-Tillman, S. Korourian, and V. S. Klimberg, *Intraoperative ultrasound-guided breast biopsy.* Am. J. Surg., 2000. **180**(6): p. 419-423.

[11] R. A. Graham, M. J. Homer, C. J. Sigler, H. Safaii, C. H. Schmid, D. Marchant, and T. Smith, *The efficacy of specimen radiography in evaluating the surgical margins of impalpable breast carcinoma.* Am. J. Roentgenol., 1994. **162**(1): p. 33-36.

[12] M. Morrow, E. A. Strom, L. W. Bassett, D. D. Dershaw, B. Fowble, A. Giuliano, J. R. Harris, F. O'Malley, S. J. Schnitt, and S. E. Singletary, *Standard for breast conservation therapy in the management of invasive breast carcinoma.* CA Cancer J. Clin., 2002. **52**(5): p. 277-300.

[13] J. K. Harness, A. E. Giuliano, B. A. Pockaj, and E. Downs-Kelly, *Margins: A status report from the annual meeting of the American society of breast surgeons.* Ann. Surg. Oncol., 2014. **21**(10): p. 3192-3197.

[14] D. T. Butcher, T. Alliston, and V. M. Weaver, *A tense situation: Forcing tumour progression.* Nat. Rev. Cancer, 2009. **9**(2): p. 108-122.

[15] S. T. Philipp, T. Kalisch, T. Wachtler, and H. R. Dinse, *Enhanced tactile acuity through mental states.* Sci. Rep., 2015. **5**: p. 13549.

[16] L. S. Bickley, P. G. Szilagyi, and B. Bates, *Bates' guide to physical examination and history taking*. 10th ed. 2009, Philadelphia: Wolters Kluwer Health/Lippincott Williams & Wilkins.

[17] A. C. Grant, R. Fernandez, P. Shilian, E. Yanni, and M. A. Hill, *Tactile spatial acuity differs between fingers: A study comparing two testing paradigms.* Atten. Percept. Psychophys., 2006. **68**(8): p. 1359-1362.

[18] R. W. Van Boven, R. H. Hamilton, T. Kauffman, J. P. Keenan, and A. Pascual–Leone, *Tactile spatial resolution in blind braille readers.* Neurology, 2000. **54**(12): p. 2230-2236.

[19] R. W. Van Boven and K. O. Johnson, *The limit of tactile spatial resolution in humans grating orientation discrimination at the lip, tongue, and finger.* Neurology, 1994. **44**(12): p. 2361-2366.

[20] L. Skedung, M. Arvidsson, J. Y. Chung, C. M. Stafford, B. Berglund, and M. W. Rutland, *Feeling small: Exploring the tactile perception limits.* Sci. Rep., 2013. **3**: p. 2617.

[21] J. A. Woods, L. F. Leslie, D. B. Drake, and R. F. Edlich, *Effect of puncture resistant surgical gloves, finger guards, and glove liners on cutaneous sensibility and surgical psychomotor skills.* J. Biomed. Mater. Res., 1996. **33**(1): p. 47-51.

[22] R. G. Pleijhuis, M. Graafland, J. De Vries, J. Bart, J. S. De Jong, and G. M. Van Dam, *Obtaining adequate surgical margins in breast-conserving therapy for patients with early-stage breast cancer: Current modalities and future directions.* Ann. Surg. Oncol., 2009. **16**(10): p. 2717-2730.

[23] P. S. Wellman, R. D. Howe, N. Dewagan, M. A. Cundari, E. Dalton, and K. A. Kern. *Tactile imaging: A method for documenting breast masses*. in *Proceedings of the First Joint BMES/EMBS Conference*. 1999. IEEE.

[24] V. Egorov and A. P. Sarvazyan, *Mechanical imaging of the breast.* IEEE Trans. Med. Imaging, 2008. **27**(9): p. 1275-1287.

[25] R. Surapaneni, Q. Guo, Y. Xie, D. J. Young, and C. H. Mastrangelo, *A three-axis high-resolution capacitive tactile imager system based on floating comb electrodes.* J. Micromechanics Microengineering, 2013. **23**(7): p. 075004.

[26] V. Egorov, S. Ayrapetyan, and A. P. Sarvazyan, *Prostate mechanical imaging: 3D image composition and feature calculations.* IEEE Trans. Med. Imaging, 2006. **25**(10): p. 1329-1340.

[27] V. Egorov, H. Van Raalte, and A. P. Sarvazyan, *Vaginal tactile imaging.* IEEE Trans. Biomed. Eng., 2010. **57**(7): p. 1736-1744.

[28] M. I. Tiwana, S. J. Redmond, and N. H. Lovell, *A review of tactile sensing technologies with applications in biomedical engineering.* Sensors and Actuators A: physical, 2012. **179**: p. 17-31.

[29] C. Pan, L. Dong, G. Zhu, S. Niu, R. Yu, Q. Yang, Y. Liu, and Z. L. Wang, *High-resolution electroluminescent imaging of pressure distribution using a piezoelectric nanowire led array.* Nat. Photonics, 2013. **7**(9): p. 752-758.

[30] A. Sahu, F. Saleheen, V. Oleksyuk, C. Mcgoverin, N. Pleshko, A. H. H. N. Torbati, J. Picone, K. Sorenmo, and C.-H. Won, *Characterization of mammary tumors using noninvasive tactile and hyperspectral sensors.* IEEE Sens. J., 2014. **14**(10): p. 3337-3344.

[31] J.-H. Lee, Y. N. Kim, and H.-J. Park, *Bio-optics based sensation imaging for breast tumor detection using tissue characterization.* Sensors, 2015. **15**(3): p. 6306-6323.

[32] S. Es'haghian, K. M. Kennedy, P. Gong, D. D. Sampson, R. A. Mclaughlin, and B. F. Kennedy, *Optical palpation in vivo: Imaging human skin lesions using mechanical contrast.* J. Biomed. Opt., 2015. **20**(1): p. 016013.

[33] K. M. Kennedy, S. Es'haghian, L. Chin, R. A. Mclaughlin, D. D. Sampson, and B. F. Kennedy, *Optical palpation: Optical coherence tomography-based tactile imaging using a compliant sensor.* Opt. Lett., 2014. **39**(10): p. 3014-3017.

[34] C. Gentle, *Mammobarography: A possible method of mass breast screening.* Med. Eng. Phys., 1988. **10**(2): p. 124-126.

[35] P. Wijesinghe, D. D. Sampson, and B. F. Kennedy, *Computational optical palpation: A finite-element approach to micro-scale tactile imaging using a compliant sensor.* J. R. Soc. Interface, 2017. **14**(128): p. 20160878.

[36] W. M. Allen, K. M. Kennedy, Q. Fang, L. Chin, A. Curatolo, L. Watts, R. Zilkens, S. L. Chin, B. F. Dessauvagie, B. Latham, C. M. Saunders, and B. F. Kennedy, *Wide-*

field quantitative micro-elastography of human breast tissue. Biomed. Opt. Express, 2018. **9**(3): p. 1082-1096.

[37] K. M. Kennedy, L. Chin, R. A. Mclaughlin, B. Latham, C. M. Saunders, D. D. Sampson, and B. F. Kennedy, *Quantitative micro-elastography: Imaging of tissue elasticity using compression optical coherence elastography.* Sci. Rep., 2015. **5**: p. 15538.

[38] W. M. Allen, P. Wijesinghe, B. F. Dessauvagie, B. Latham, C. M. Saunders, and B. F. Kennedy, *Optical palpation for the visualization of tumor in human breast tissue.* J. Biophotonics, 2018. **X**(YY): p. ZZ-ZZ. See online supporting information.

[39] G. Lamouche, B. F. Kennedy, K. M. Kennedy, C.-E. Bisaillon, A. Curatolo, G. Campbell, V. Pazos, and D. D. Sampson, *Review of tissue simulating phantoms with controllable optical, mechanical and structural properties for use in optical coherence tomography.* Biomed. Opt. Express, 2012. **3**(6): p. 1381-1398.

[40] B. F. Kennedy, S. H. Koh, R. A. Mclaughlin, K. M. Kennedy, P. R. T. Munro, and D. D. Sampson, *Strain estimation in phase-sensitive optical coherence elastography.* Biomed. Opt. Express, 2012. **3**(8): p. 1865-1879.

[41] J. Canny, *A computational approach to edge detection.* IEEE Trans. Pattern. Anal. Mach. Intell., 1986. **PAMI-8**(6): p. 679-698.

[42] L. Scolaro, R. A. Mclaughlin, B. F. Kennedy, C. M. Saunders, and D. D. Sampson, *A review of optical coherence tomography in breast cancer.* Photonics Lasers Med., 2014. **3**(3): p. 225-240.

[43] F. T. Nguyen, A. M. Zysk, E. J. Chaney, J. G. Kotynek, U. J. Oliphant, F. J. Bellafiore, K. M. Rowland, P. A. Johnson, and S. A. Boppart, *Intraoperative evaluation of breast tumor margins with optical coherence tomography.* Cancer Res., 2009. **69**(22): p. 8790-8796.

[44] C. Zhou, D. W. Cohen, Y. Wang, H.-C. Lee, A. E. Mondelblatt, T.-H. Tsai, A. D. Aguirre, J. G. Fujimoto, and J. L. Connolly, *Integrated optical coherence tomography and microscopy for ex vivo multiscale evaluation of human breast tissues.* Cancer Res., 2010. **70**(24): p. 10071-10079.

[45] S. Es'haghian, K. M. Kennedy, P. Gong, Q. Li, L. Chin, P. Wijesinghe, D. D. Sampson, R. A. Mclaughlin, and B. F. Kennedy, *In vivo volumetric quantitative micro-elastography of human skin.* Biomed. Opt. Express, 2017. **8**(5): p. 2458-2471.

[46] L. Dong, P. Wijesinghe, J. T. Dantuono, D. D. Sampson, P. R. Munro, B. F. Kennedy, and A. A. Oberai, *Quantitative compression optical coherence elastography as an inverse elasticity problem.* IEEE J. Sel. Topics Quantum Electron., 2016. **22**(3): p. 277-287.

Figure 1. Comparison of optical palpation and QME. (a) Schematic of the loading stages of a sample with a stiff inclusion, (i) undeformed, (ii) with preload applied, resulting in a layer preload strain, $\mu_{layer,P}$, and (iii) with actuation applied, resulting in local strain in the layer, $\mu_{layer,L}$, and sample, $\mu_{sample,L}$. (b) Optical palpation: the layer preload stress, $\tilde{A}_{layer,P}$, is estimated by relating the layer preload strain to the stress-strain response of the layer, E_{layer}. (c) QME: the sample elasticity, E_{sample}, is estimated by relating the layer local stress, $\tilde{A}_{layer,L}$ to the sample local strain, $\mu_{sample,L}$.

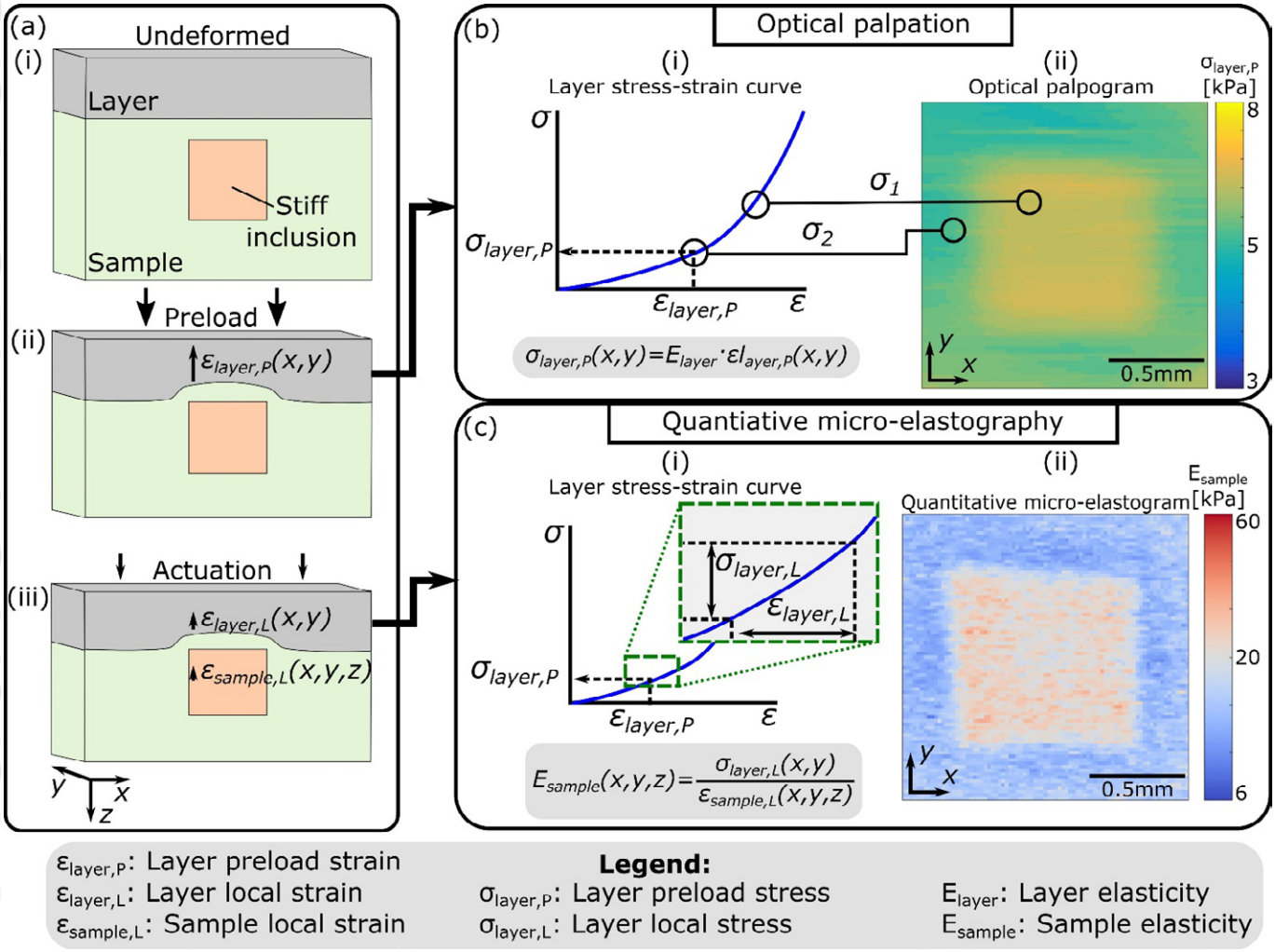

Figure 2. Optical palpation of a freshly excised mastectomy specimen containing invasive tumor. (a) Photograph of the preloaded specimen. (b) Low magnification histology. (c) High magnification histology. Wide-field *en face* (d) OCT image and (e) optical palpogram. Magnified *en face* (f) OCT image and (g) optical palpogram. A, Adipose tissue; S, Uninvolved stroma; T, Invasive tumor.

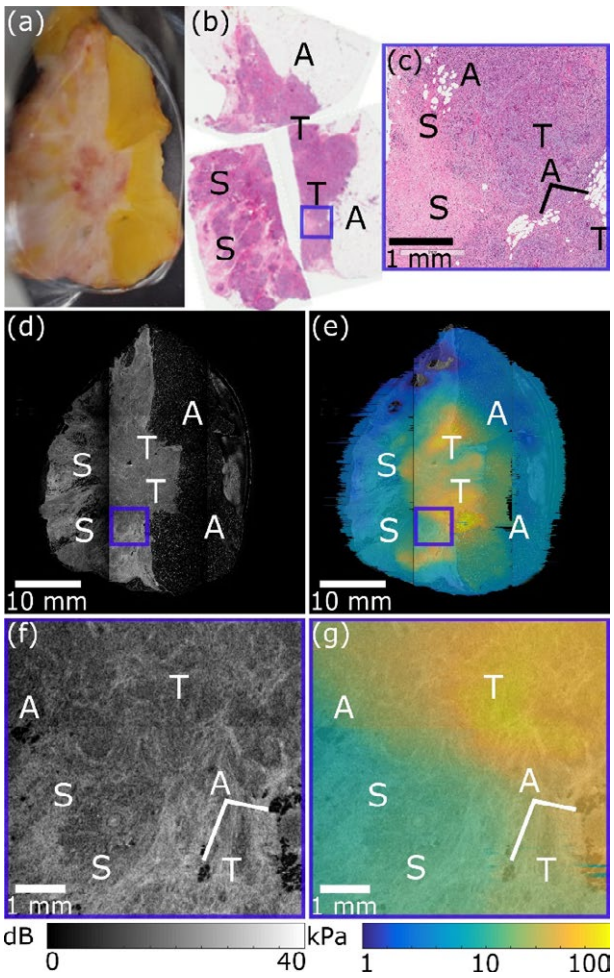

Figure 3. Optical palpation of breast-conserving surgery specimen with a margin involved by invasive tumor. (a) Photograph of the specimen. (b) Histology. Wide-field *en face* (c) OCT image and (d) optical palpogram. Magnified *en face* (e) OCT image and (f) optical palpogram. A, Adipose tissue; L, Layer artifact; S, Stroma; T, Invasive tumor. The direction of OCT beam indicated by black arrows in (b). Digital micrograph in the plane orthogonal to *en face* images, the approximate location indicated by the red dashed line in (c)-(f).

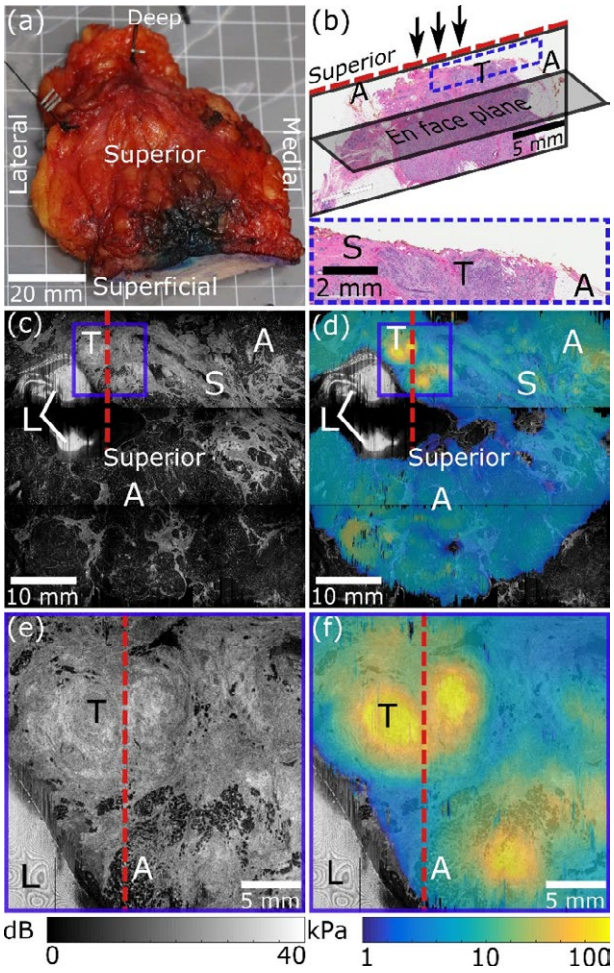

Figure 4. Optical palpation of a benign fibroadenoma excised during breast-conserving surgery. (a) Photograph of the specimen. (b) Representative histology. Wide-field *en face* (c) OCT image and (d) optical palpogram. Magnified *en face* (e) OCT image and (f) optical palpogram. A, Adipose tissue; FA, Benign fibroadenoma; L, Layer artifact.

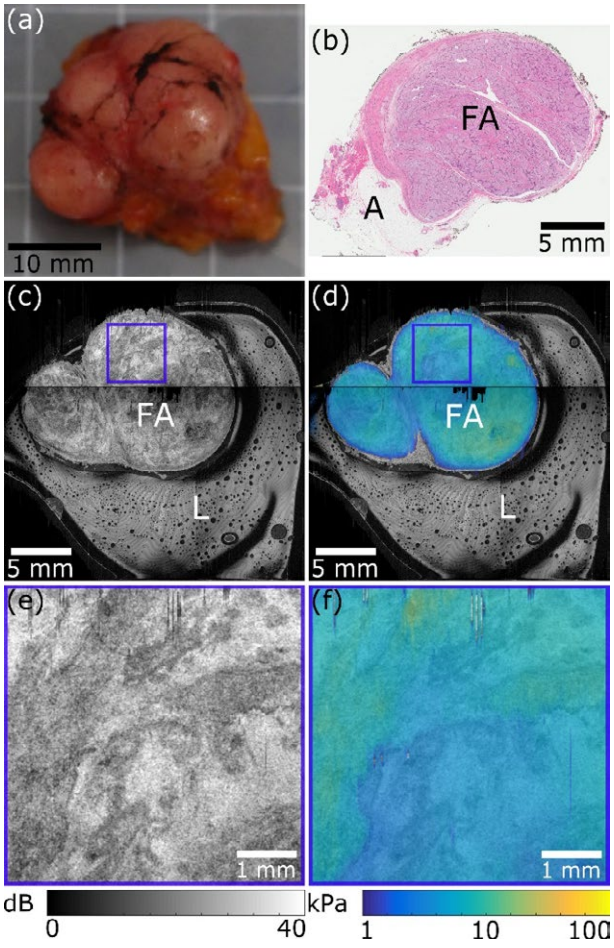

Figure 5. Comparison of OCT, optical palpation and QME of a freshly excised mastectomy specimen containing high-grade ductal carcinoma *in situ* (DCIS). (a) Photograph of specimen excised from a mastectomy. (b) Low magnification histology. (c) High magnification histology. Wide-field *en face* (d) OCT image, (e) optical palpogram and (f) quantitative micro-elastogram. Magnified *en face* (g) OCT image, (h) optical palpogram and (i) quantitative micro-elastogram. A, Adipose tissue; D, DCIS; FC, Focal calcifications; W, Duct walls.

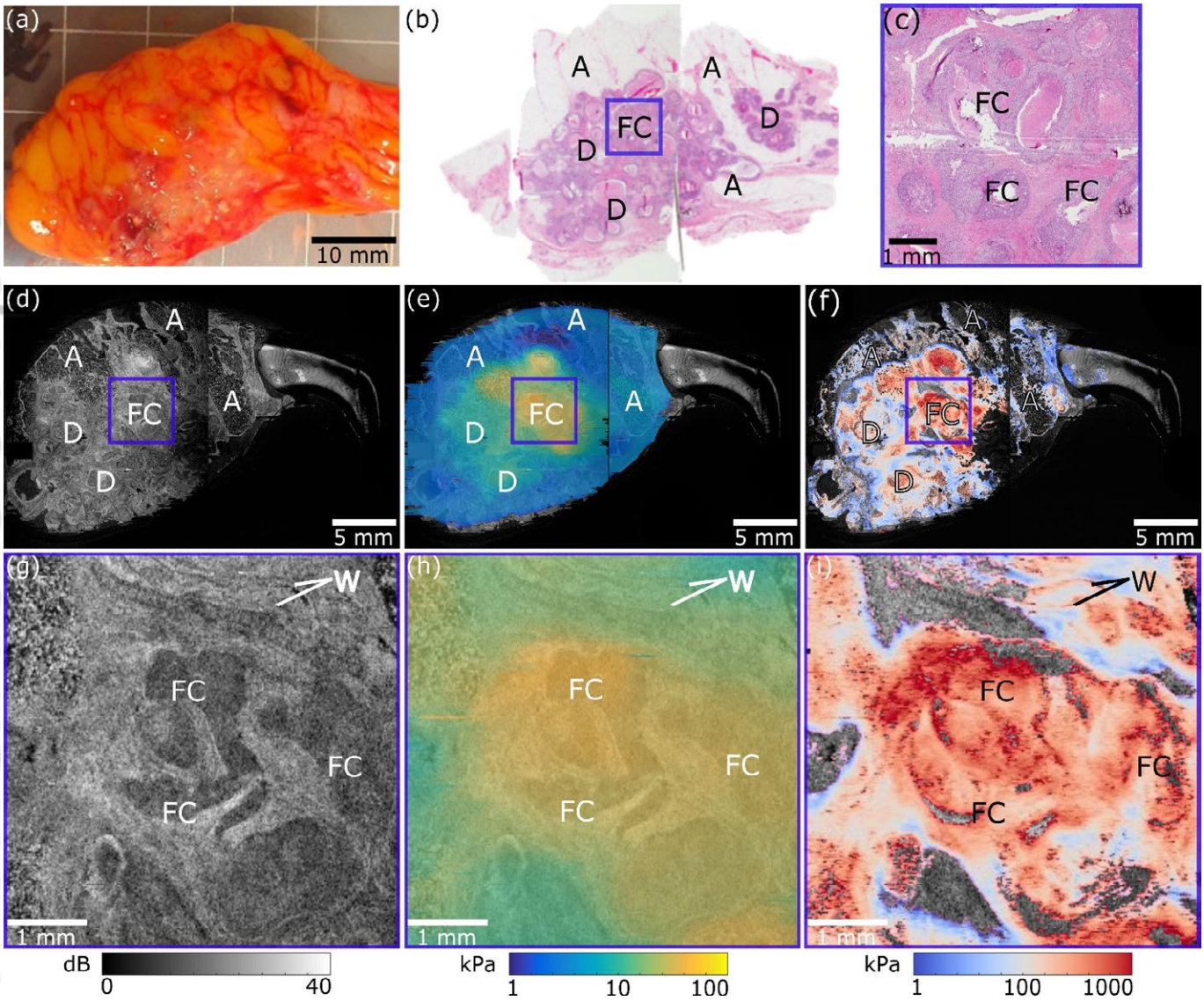

Figure 6. Mean stress for adipose tissue, uninvolved dense tissue and invasive tumor, represented as box plots, showing the statistically significant higher stress for invasive tumor in comparison to adipose tissue and uninvolved dense tissue (***p <0.001). The horizontal red line indicates the median. The blue box indicates the interquartile range. The whiskers represent the range of measurements within the 1.5× interquartile range. The red addition sign represents outliers. The solid black circles represent the mean.